JOURNAL OF SPACECRAFT AND ROCKETS
Vol. 37, No. 3, May–June 2000

Effect of Face-Sheet Anisotropy on Buckling and Postbuckling of Sandwich Plates

Terry Hause*
Virginia Polytechnic Institute and State University, Blacksburg, Virginia 24061
Theodore F. Johnson†
NASA Langley Research Center, Hampton, Virginia 23081-0001
and
Liviu Librescu‡
Virginia Polytechnic Institute and State University, Blacksburg, Virginia 24061

A study of the effect of anisotropy of face sheets on buckling and postbuckling of sandwich flat panels subjected to both mechanical and thermal loads is presented. The mechanical loads consist of uniaxial compressive/tensile edge loads, while the temperature is assumed to exhibit an antisymmetric variation through the panel thickness. The study is carried out in the context of a geometrically nonlinear theory of sandwich structures that also incorporates the effect of unavoidable stress-free initial geometric imperfections. A detailed analysis of the influence of a large number of parameters associated with the panel geometry, material properties of the core, fiber orientation and stacking sequence in the face sheet, and character of tangential boundary conditions (i.e., movable or immovable) on buckling strength and postbuckling response is accomplished, and pertinent conclusions are outlined.

Nomenclature

a = distance between the global midsurface and the midsurface of facings
E_1, E_2 = in-plane Young's moduli, Msi
e_{ij} = three-dimensional strain tensor
G_{12}, $\bar{G}_{13}$, $\bar{G}_{23}$ = in-plane shear modulus of material of face sheets; transverse shear moduli of the core, Msi
h_p, h, $\bar{h}$, H = thickness of each constitent ply of face-sheets, thickness of the facings, thickness of the core, and total thickness of the structure, respectively
L_1, L_2 = panel length and width, respectively
N = number of layers in the upper facings, equal to that in the bottom facings
$\bar{N}_{13}$, $\bar{N}_{23}$ = transverse shear stress resultants associated with the core
q_3, q_{pq} = transverse load and its modal amplitudes, respectively
S_{ij} = second Piola–Kirchhoff stress tensor
$T(x_1, x_2, x_3)$, $\overset{1}{T}(x_1, x_2)$, $\overset{1}{T}_{pq}$ = three-dimensional temperature field, thickness temperature distribution and its modal amplitudes, respectively
$T_u(x_1, x_2)$, $T_b(x_1, x_2)$ = temperature distributions on the top and bottom faces of the sandwich panel, respectively
V_α, V_3 = three-dimensional tangential and transversal displacement components
$\overset{\circ}{V}{}'_\alpha$, $\overset{\circ}{V}{}''_\alpha$ = tangential displacement components of points of midplanes of the bottom and top face sheets, respectively
v_3, $\overset{\circ}{v}_3$; w_{mn}, $\overset{\circ}{w}_{mn}$ = deflection, initial geometric imperfection; their modal amplitudes, respectively
x_α, x_3 = tangential and thicknesswise coordinates, respectively
Δ_1 = end shortening in the x_1 direction
ϵ_{ij} = two-dimensional strain measures
λ_m, μ_n = $m\pi/L_1$, $n\pi/L_2$, $(m, n = 1, 2, \ldots)$
$\lambda_{\alpha\beta}$, $\hat{\lambda}_{\alpha\beta}$ = thermal compliance expansion coefficients and their modified counterparts, respectively
ξ_α, η_α = two-dimensional tangential displacement measures
ψ = panel aspect ratio ($\equiv L_2/L_1$)

Subscripts

$(\cdot)_f$, $(\cdot)_c$ = quantities associated with the face and core layers, respectively
$(\cdot)$, i = $\partial(\cdot)/\partial x_i$
$(\cdot)_n$, $(\cdot)_t$ = normal and tangential in-plane directions to an edge, implying ($n = 1$, $t = 2$) or ($n = 2$, $t = 1$)
$\underset{\sim}{(\cdot)}$ = prescribed quantity

Superscripts

$(\cdot)'$, $(\cdot)''$, $(\bar{\cdot})$ = quantities affiliated with the bottom face sheets, upper face sheets, and core layer, respectively

Introduction

A RENEWED interest in the use of sandwich structures in the construction of advanced supersonic/hypersonic flight vehicles and reusable space transportion systems has been demonstrated in the last decade. Some of the underlying reasons and motivation for this interest are, among others, 1) the possibility to integrate the advanced fiber-reinforced composite materials in the face sheets and the core, their use being likely to provide increased bending stiffness with little resultant weight penalty, long fatigue life, and directional properties, as well as the capability of operating in a high-temperature environment; 2) the possibility to provide thermal and sound insulation characteristics, as well as a smooth aerodynamic surface, in a higher speed flow environment; and 3) extended operational life as compared to stiffened-reinforced structures that are weakened by the appearance of stress concentration. Needless to say, the development of new manufacturing techniques that make the use of sandwich structures economically feasible has contributed heavily to the widespread use of such structures in the aerospace industry.

As is well known, any combination of biaxial loading and external pressure can be found in a typical aircraft structure. Moreover, high-speed and launch vehicles are likely to be exposed during their missions to severe temperature fields. In such a context, development of a comprehensive structural model of sandwich flat panels

Received 10 March 1999; revision received 2 September 1999; accepted for publication 12 December 1999.

*Engineer, Engineering Science and Mechanics Department.
†Aerospace Engineer, Thermal Structures Branch.
‡Professor, Engineering Science and Mechanics Department.

and of adequate computational methodologies able to address problems of determination of their buckling strength and load-bearing capabilities in the nonlinear range represent issues of practical importance in the design of such structures.

One of the goals of the paper is to develop a rather comprehensive theory of sandwich flat panels incorporating geometric nonlinearities in the von Kármán sense, the initial geometric imperfection, and the directionality property of the materials of face sheet. In particular, the directional property of fibrous composites can be used to enhance the buckling strength and the load-carrying capacity in the nonlinear range. In spite of the available literature devoted to the modeling and analysis of flat sandwich panels with laminated face sheets (for example, see Ref. 1, which is the most recent and comprehensive review of the state of the art in the field of sandwich structures), to the best of the authors' knowledge, the problem of the enhancement of the load-carrying capacity of flat sandwich panels in both linear and nonlinear ranges using the tailorability property of laminated face sheets has not yet been addressed. For special cases related to linear stability problems, a number of results can be found in Refs. 2–7.

To be reasonably self-contained, in the following section, the basic equations of sandwich plate theory incorporating geometric nonlinearities, initial geometric imperfections, anisotropy of the individual face sheets, and transverse shear effects in the core layer are displayed only to the extent that they are needed in the treatment of the subject considered in this paper.

Basic Assumptions and Conventions

The global middle plane of the structure σ, selected to coincide with that of the core layer, is referred to an curvilinear and orthogonal coordinate system x_α, where $\alpha = 1, 2$. The through-the-thickness coordinate x_3 is considered positive when measured in the direction of the inward normal. Consistent with the convention given in the Nomenclature, the uniform thickness of the core is $2\bar{h}$, whereas those of the upper and bottom face sheets as h'' and h', respectively. As a result, $H(\equiv 2\bar{h} + h' + h'')$ is the total thickness of the structure (Fig. 1).

Toward developing the geometrically nonlinear theory of sandwich flat panels, the following assumptions are adopted:

1) The face sheets are composed of a number of orthrotropic material laminas, the axes of orthrotropy of the individual plies being rotated with respect to the geometrical axes x_α of the structure.

2) The material of the core features orthotropic properties, the axes of orthotropy being parallel to the geometrical axes x_α.

3) The core layer is capable of carrying transverse shear stresses only, in which case we deal with a weak core.

4) A perfect bonding between the face sheets and the core and between the constituent laminas of the face sheets is assumed to be valid.

5) The assumption of incompressibility in the transverse normal direction is adopted for both the core and face sheets.

6) The layers constituting the faces are assumed to be thin, and as a result, transverse shear effects are neglected in the face sheets.

7) The structure as a whole, as well as both the top and bottom laminated face sheets, is assumed to exhibit mechanical and geometrical symmetry properties with respect to both the midplane of the core layer and about their own midplanes as well.

8) The geometrical nonlinearities are considered in the von Kármán sense; this implies that the nonlinearities associated with tangential displacements are small as compared with those associated with transversal deflection.

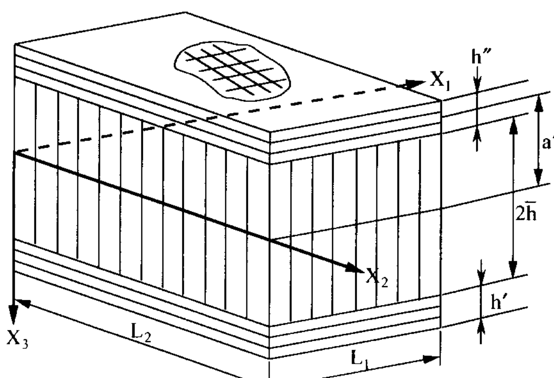

Fig. 1 Sandwich flat panel element.

Kinematics

Several basic kinematic relationships derived in Refs. 8 and 9 will be supplied.

Three-Dimensional Displacement Field in the Face Sheets and Core

In agreement with the stipulated assumptions, the transverse displacement should be uniform through the thickness of the laminate, which implies

$$V_3'(x_1, x_2, x_3) = V_3''(x_1, x_2, x_3) = \bar{V}_3(x_1, x_2, x_3) \equiv v_3(x_1, x_2) \quad (1)$$

When the transverse shear effects in the face sheets are discarded, the three-dimensional distribution of the displacement field fulfilling the kinematic continuity conditions at the interfaces between the core and facings results as[8,9]

$$V_1'(x_\alpha, x_3) = \xi_1(x_\alpha) + \eta_1(x_\alpha) - (x_3 - a)\frac{\partial v_3(x_\alpha)}{\partial x_1} \quad (2a)$$

$$V_2'(x_\alpha, x_3) = \xi_2(x_\alpha) + \eta_2(x_\alpha) - (x_3 - a)\frac{\partial v_3(x_\alpha)}{\partial x_2}$$

$$(\bar{h} \le x_3 \le \bar{h} + h') \quad (2b)$$

$$V_3'(x_\alpha, x_3) = v_3(x_\alpha) \quad (2c)$$

$$\bar{V}_1(x_\alpha, x_3) = \xi_1(x_\alpha) + \left(\frac{x_3}{\bar{h}}\right)\left\{\eta_1(x_\alpha) + \left(\frac{h}{2}\right)\frac{\partial v_3(x_\alpha)}{\partial x_1}\right\} \quad (3a)$$

$$\bar{V}_2(x_\alpha, x_3) = \xi_2(x_\alpha) + \left(\frac{x_3}{\bar{h}}\right)\left\{\eta_2(x_\alpha) + \left(\frac{h}{2}\right)\frac{\partial v_3(x_\alpha)}{\partial x_2}\right\}$$

$$(-\bar{h} \le x_3 \le \bar{h}) \quad (3b)$$

$$\bar{V}_3(x_\alpha, x_3) = v_3(x_\alpha) \quad (3c)$$

$$V_1''(x_\alpha, x_3) = \xi_1(x_\alpha) - \eta_1(x_\alpha) - (x_3 + a)\frac{\partial v_3(x_\alpha)}{\partial x_1} \quad (4a)$$

$$V_2''(x_\alpha, x_3) = \xi_2(x_2) - \eta_2(x_\alpha) - (x_3 + a)\frac{\partial v_3(x_\alpha)}{\partial x_2}$$

$$(-\bar{h} - h'' \le x_3 \le -\bar{h}) \quad (4b)$$

$$V_3''(x_\alpha, x_3) = v_3(x_\alpha) \quad (4c)$$

In these equations, $V_i(x_\alpha, x_3)$ are the three-dimensional displacement components in the directions of the coordinates x_i.

In addition,

$$\xi_\alpha = (\mathring{V}'_\alpha + \mathring{V}''_\alpha)/2 \quad (4d)$$

$$\eta_\alpha = (\mathring{V}'_\alpha - \mathring{V}''_\alpha)/2 \quad (4e)$$

are the two-dimensional tangential modified displacement measures, where $\mathring{V}'_\alpha$ and $\mathring{V}''_\alpha$ are the tangential displacements of the points of the midplanes of the bottom and top face sheets, respectively. For a symmetric sandwich panel, $h' = h'' \equiv h$ define the thickness of the bottom and top face sheets, whereas $a' = a'' = a(\equiv \bar{h} + h/2)$ are the distances between the global midplane of the structure and the midplanes of the bottom and top face sheets, respectively. Henceforth, the Greek indices have the range 1, 2, whereas the Latin indices have the range 1 through 3, and unless otherwise stated, the Einstein summation convention over the repeated indices is employed.

Distribution of Strains Across the Thickness of the Sandwich Panel

It is assumed that the structure features a stress-free small initial geometric imperfection $\overset{\circ}{V}_3 [\equiv \overset{\circ}{v}_3(x_\alpha)]$. By the adoption of the concept of small strains and moderately small rotations, referred to as the von Kármán assumption,[10–12] the components of the three-dimensional Lagrangian strain tensor e_{ij} result as follows.

In the bottom face sheets,

$$'e_{11} = '\varepsilon_{11} + (x_3 - a')\kappa'_{11} \tag{5a}$$

$$'e_{22} = '\varepsilon_{22} + (x_3 - a')\kappa'_{22} \qquad (\bar{h} \le x_3 \le \bar{h} + h') \tag{5b}$$

$$2'e_{12} = '\gamma_{12} + (x_3 - a')\kappa'_{12} \tag{5c}$$

In the core layer,

$$\bar{e}_{11} = \bar{\varepsilon}_{11} + x_3\bar{\kappa}_{11} \tag{6a}$$

$$\bar{e}_{22} = \bar{\varepsilon}_{22} + x_3\bar{\kappa}_{22} \qquad (-\bar{h} \le x_3 \le \bar{h}) \tag{6b}$$

$$2\bar{e}_{12} = \bar{\gamma}_{12} + x_3\bar{\kappa}_{12} \tag{6c}$$

$$2\bar{e}_{13} = \bar{\gamma}_{13} \tag{6d}$$

$$2\bar{e}_{23} = \bar{\gamma}_{23} \tag{6e}$$

In the upper face sheets,

$$''e_{11} = ''\varepsilon_{11} + (x_3 + a'')\kappa''_{11} \tag{7a}$$

$$''e_{22} = ''\varepsilon_{22} + (x_3 + a'')\kappa''_{22} \qquad (-\bar{h} - h'' \le x_3 \le -\bar{h}) \tag{7b}$$

$$2''e_{12} = ''\gamma_{12} + (x_3 + a'')\kappa''_{12} \tag{7c}$$

In these equations, ε_{11}, ε_{22}, and $\varepsilon_{12}(\equiv \gamma_{12}/2)$ and $\varepsilon_{13}(\equiv \gamma_{13}/2)$ and $\varepsilon_{23}(\equiv \gamma_{23}/2)$ are the two-dimensional tangential and the transverse shear strain measures, respectively. The expressions of the two-dimensional strain measures in terms of the two-dimensional displacement quantities are displayed in the Appendix. Note that Eqs. (6a–6e) are applicable in general to strong core sandwich structures. For the weak core sandwich structures, only Eqs. (6d) and (6e) are relevant.

Governing Equations

The governing equations for the geometrically nonlinear theory of sandwich flat panels are represented in terms of displacement quantities.

In spite of the intricacy, this formulation is not subjected to any restriction related to the anisotropy of the core and faces or the nature of the core (weak or strong).

As a preliminary step, the principle of virtual work is used to derive the two-dimensional equations of equilibrium of the theory of sandwich structures and the associated boundary conditions. According to this principle,

$$\delta J = \delta(U - W) = 0 \tag{8}$$

where U is the strain energy, W is the work done by surface tractions and edge loads, and δ is the variation operator. Incorporating the effect of a temperature field, and assuming materials exhibiting monoclinic symmetry in the face sheets, consistent with the model of weak core sandwich structures, we have

$$\begin{aligned}\delta U = \frac{1}{2}\delta\int_\sigma \Bigg\{ &\int_{\bar{h}}^{\bar{h}+\bar{h}'} (\hat{Q}'_{\alpha\beta\omega\rho} e'_{\alpha\beta} e'_{\omega\rho} - 2\hat{\lambda}'_{\alpha\beta} T e'_{\alpha\beta})\,\mathrm{d}x_3 \\ &+ \int_{-\bar{h}-h''}^{-\bar{h}} (\hat{Q}''_{\alpha\beta\omega\rho} e''_{\alpha\beta} e''_{\omega\rho} - 2\hat{\lambda}''_{\alpha\beta} T e''_{\alpha\beta})\,\mathrm{d}x_3 \\ &+ \int_{-\bar{h}}^{\bar{h}} \bar{Q}_{\alpha3\omega3}\bar{e}_{\alpha3}\bar{e}_{\omega3})\,\mathrm{d}x_3 \Bigg\}\,\mathrm{d}\sigma\end{aligned} \tag{9}$$

whereas

$$\delta W = \int_{\Omega_s} \underset{\sim}{S}_i \delta V_i \,\mathrm{d}\Omega \tag{10}$$

In these equations $\underset{\sim}{S}_i = \underset{\sim}{S}_{ij} n_j$ are the components of the stress vector defined on that part Ω_s of the external boundary Ω where stresses are prescribed, S_{ij} is the second Piola–Kirchhoff stress tensor, n_i are the components of the outward unit vector normal to Ω, σ is the undeformed midplane of the sandwich panel, and $T[\equiv T(x_\alpha, x_3)]$ is the rise of the temperature above a stress-free reference temperature T_o. In addition,[10]

$$\hat{Q}_{\alpha\beta\omega\rho}\left(\equiv Q_{\alpha\beta\omega\rho} - \frac{Q_{\alpha\beta33}Q_{33\omega\rho}}{Q_{3333}}\right) \tag{11a}$$

$$\hat{\lambda}_{\alpha\beta}\left(\equiv \lambda_{\alpha\beta} - \frac{Q_{\alpha\beta33}}{Q_{3333}}\lambda_{33}\right) \tag{11b}$$

are the modified elastic moduli and thermal compliance coefficients, respectively. Within this study one assumes that Q_{ijmn} and λ_{ij} are temperature-independent elastic and thermal expansion coefficients. Replacement of Eqs. (9) and (10) and of (6–9) in Eq. (8), carrying out the integration with respect to x_3, integrating by parts wherever necessary to relieve the virtual displacements of any differentiation, and invoking the arbitrary character of the variations $\delta\eta_1$, $\delta\eta_2$, $\delta\xi_1$, $\delta\xi_2$, and δv_3 throughout the entire domain of the plate by setting to zero the coefficients of these variations, one obtains the five equations of equilibrium and the associated boundary conditions valid for the theory of weak core sandwich structures.

The equations of equilibrium are

$$\delta\xi_1\colon N_{11,1} + N_{12,2} = 0 \tag{12a}$$

$$\delta\xi_2\colon N_{22,2} + N_{12,1} = 0 \tag{12b}$$

$$\delta\eta_1\colon L_{11,1} + L_{12,2} - \bar{N}_{13} = 0 \tag{12c}$$

$$\delta\eta_2\colon L_{22,2} + L_{12,1} - \bar{N}_{23} = 0 \tag{12d}$$

$$\begin{aligned}\delta v_3\colon & N_{11}(v_{3,11} + \overset{\circ}{v}_{3,11}) + 2N_{12}(v_{3,12} + \overset{\circ}{v}_{3,12}) \\ &+ N_{22}(v_{3,22} + \overset{\circ}{v}_{3,22}) + (M_{11,11} + 2M_{12,12} \\ &+ M_{22,22}) + a/\bar{h}(\bar{N}_{13,1} + \bar{N}_{23,2}) + q_3 = 0\end{aligned} \tag{12e}$$

In addition, the boundary conditions that result are

$$N_{nn} = \underset{\sim}{N}_{nn} \qquad \text{or} \qquad \xi_n = \underset{\sim}{\xi}_n \tag{13a}$$

$$N_{nt} = \underset{\sim}{N}_{nt} \qquad \text{or} \qquad \xi_t = \underset{\sim}{\xi}_t \tag{13b}$$

$$L_{nn} = \underset{\sim}{L}_{nn} \qquad \text{or} \qquad \eta_n = \underset{\sim}{\eta}_n, \qquad \underset{n,t}{\not{\sum}} \tag{13c}$$

$$L_{nt} = \underset{\sim}{L}_{nt} \qquad \text{or} \qquad \eta_t = \underset{\sim}{\eta}_t \tag{13d}$$

$$M_{nn} = \underset{\sim}{M}_{nn} \qquad \text{or} \qquad v_{3,n} = \underset{\sim}{v}_{3,n} \tag{13e}$$

$$\begin{aligned}&N_{nt}(v_{3,t} + \overset{\circ}{v}_{3,t}) + N_{nn}(v_{3,n} + \overset{\circ}{v}_{3,n}) + M_{nn,n} + 2M_{nt,t} \\ &\quad + (a/\bar{h})\bar{N}_{n3} = \underset{\sim}{M}_{nt,t} + \underset{\sim}{\bar{N}}_{n3} \qquad \text{or} \qquad v_3 = \underset{\sim}{v}_3\end{aligned} \tag{13f}$$

where the subscripts n and t are used to designate the normal and tangential in-plane directions to an edge and, hence, $n = 1$ when $t = 2$, and vice versa. In addition, the sign

$$\underset{n,t}{\not{\sum}}$$

indicates that no summation over the indices n and t is implied. The earlier displayed equations of equilibrium and static boundary conditions are expressed in terms of the global stress resultants and stress couples as

$$N_{11} = N'_{11} + N''_{11} \qquad (1 \Leftrightarrow 2) \tag{14a}$$

$$N_{12} = N'_{12} + N''_{12} \tag{14b}$$

$$L_{11} = \bar{h}(N'_{11} - N''_{11}) \qquad (1 \Leftrightarrow 2) \tag{14c}$$

$$L_{12} = \bar{h}(N'_{12} - N''_{12}) \tag{14d}$$

$$M_{11} = M'_{11} + M''_{11} \qquad (1 \Leftrightarrow 2) \tag{14e}$$

$$M_{12} = M'_{12} + M''_{12} \tag{14f}$$

where $(N'_{\alpha\beta}, M'_{\alpha\beta})$, $(N''_{\alpha\beta})$, and $\bar{N}_{\alpha 3}$ are the stress resultants and stress couples associated with the lower and upper face sheets and with the core layer, respectively. These quantities are defined as

$$\{N'_{\alpha\beta}, M'_{\alpha\beta}\} = \sum_{k=1}^{N} \int_{(x_3)_{k-1}}^{(x_3)_k} (S'_{\alpha\beta})_k \{1, x_3 - a\} \,\mathrm{d}x_3 \tag{15a}$$

$$\bar{N}_{\alpha 3} = \int_{-\bar{h}}^{\bar{h}} \bar{S}_{\alpha 3} \,\mathrm{d}x_3 \qquad (\alpha, \beta = 1, 2) \tag{15b}$$

The sign $(1 \Leftrightarrow 2)$ indicates that, from the equations accompanied by this sign, companion equations, not explicitly displayed, can be obtained by replacing subscript 1 by 2, and vice versa. In addition, N is the number of layers in the bottom face sheets equal to that in the top faces, whereas $(x_3)_k$ and $(x_3)_{k-1}$ are the distances from the global midplane of structure to the upper and lower interfaces of the kth layer, respectively.

Following usual procedure, replacement in the equations of equilibrium of stress resultants and stress couples expressed in terms of displacement quantities η_1, η_2, ξ_1, ξ_2, and v_3 yields the governing equations expressed in terms of these quantities.

The resulting governing equation system is of 12th-order and, consistent with this order, 6 boundary conditions must be prescribed at each panel edge. Because of their intricacy, the governing equations are not displayed here. For a version of these equations, the reader is referred to Ref. 12.

Postbuckling Equations

One of the goals of this paper is to highlight the powerful role the directionality property and layup of the face-sheet composite materials can play toward enhancing the buckling strength and postbuckling response behavior.

Two types of simply supported boundary conditions, type A and type B, are considered. Type A implies that the panel edges are simply supported and freely movable in the tangential directions to the panel midplane, normal to the panel edge. For this case the boundary conditions along the edges $x_n = 0, L_n$, are given by

$$N_{nn} = -\underset{\sim}{N}_{nn} \tag{16a}$$

$$N_{nt} = 0 \tag{16b}$$

$$\eta_n = 0 \tag{16c}$$

$$\eta_t = 0 \tag{16d}$$

$$M_{nn} = 0 \tag{16e}$$

$$v_3 = 0 \tag{16f}$$

Type B implies that all of the edges are simply supported and that the unloaded edges are immovable in the tangential plane, normal to panel edges. The boundary conditions associated with the immovable edges $x_n = 0, L_n$ are

$$\xi_n = 0 \tag{17a}$$

$$N_{nt} = 0 \tag{17b}$$

$$\eta_n = 0 \tag{17c}$$

$$\eta_t = 0 \tag{17d}$$

$$M_{nn} = 0 \tag{17e}$$

$$v_3 = 0 \tag{17f}$$

Condition (17a) is fulfilled in an average sense as

$$\int_o^{L_n} \int_o^{L_t} \left(\frac{\partial \xi_n}{\partial x_n}\right) \mathrm{d}x_n \,\mathrm{d}x_t = 0, \qquad \not\sum_{n,t} \tag{18}$$

wherefrom following the procedure described in Refs. 10, 13, and 14, the fictitious edge load $\underset{\sim}{N}_{nn}$ rendering the edges $x_n = 0, L_n$ immovable is obtained.

The boundary conditions (16a), (16b), and (17b) are fulfilled in an average sense as

$$\int_o^{L_t} N_{nn} \,\mathrm{d}x_t = -\underset{\sim}{N}_{nn} L_n \tag{19a}$$

$$\begin{pmatrix} n = 1, 2 \\ t = 2, 1 \end{pmatrix} \quad \not\sum_{n,t}$$

$$\int_o^{L_t} N_{nt} \,\mathrm{d}x_t = 0 \tag{19b}$$

where $\underset{\sim}{N}_{nn}$ are the compressive edge loads acting on the edges $x_n = 0, L_n$. Recall that in these equations n and t are the directions normal and tangential to an edge, respectively.

The transverse deflection fulfilling the kinematic boundary conditions in the transverse direction and the initial geometric imperfection yielding, in addition, the most severe postbuckling response are[15,16]

$$\begin{Bmatrix} v_3(x_1, x_2) \\ \mathring{v}_3(x_1, x_2) \end{Bmatrix} = \begin{Bmatrix} w_{pq} \\ \mathring{w}_{pq} \end{Bmatrix} \sin \lambda_p x_1 \sin \mu_q x_2 \tag{20}$$

where $\lambda_p = p\pi/L_1$, $\mu_q = q\pi/L_2$, w_{pq} and $\mathring{w}_{pq}$ are the modal amplitudes, and L_1 and L_2 are the edge lengths of the panel.

The variation of the temperature field through the panel thickness is

$$T(x_1, x_2, x_3) = x_3 \overset{1}{T}(x_1, x_2) \tag{21a}$$

where

$$\overset{1}{T}(x_1, x_2) = (T_b - T_u)/H \tag{21b}$$

$T_u [\equiv T_u(x_1, x_2)]$ and $T_b [\equiv T_b(x_1, x_2)]$ are the temperature distributions at the surfaces $x_3 = -H/2$ and $x_3 = H/2$, respectively. Such a representation of the temperature field is appropriate, for example, in the conditions occurring during the accelerated flight of a high-speed space vehicle. The temperature $\overset{1}{T}$ and the distributed lateral load q_3 are expressed as

$$\begin{Bmatrix} \overset{1}{T}(x_1, x_2) \\ q_3(x_1, x_2) \end{Bmatrix} = \begin{Bmatrix} \overset{1}{T}_{pq} \\ q_{pq} \end{Bmatrix} \sin \lambda_p x_1 \sin \mu_q x_2 \qquad (p, q = 1, 2, \ldots) \tag{22}$$

where $\overset{1}{T}_{pq}$ and q_{pq} are the temperature and lateral pressure amplitudes of modes (p,q) in the developments of $\overset{1}{T}$ and q_3, respectively.

Table 1 Material properties for the face sheets

Type	Material	E_1, Msi	E_2, Msi	G_{12}, Msi	ν_{12}	α_1, in./in./°F	α_2, in./in./°F
F1	HS graphite epoxy	26.25	1.5	1.05	0.28	6.3×10^{-6}	20.5×10^{-6}
F2	IM7/977-2	11.6	10.9	1.4	0.06	0.9×10^{-6}	0.93×10^{-6}
F3	SCS-6/Ti-15-3	27.72	18.09	8.15	0.30	——	——
F4	IM7 K3BR-4	22.0	1.2	0.6	0.30	——	——
F5	CFRP	33.22	1.936	0.761	0.32	——	——

Table 2 Material properties for the core

Type	Core type, honeycomb	$\bar{G}_{13}$, Msi	$\bar{G}_{23}$, Msi
C1	Titanium	0.20835	0.09435
C2	Aluminum	0.021177	0.0131121
C3	Aluminum	0.014200	0.008600

Using the preceding representations of $v_3(x_1, x_2)$, $\mathring{v}_3(x_1, x_2)$, and $\overset{1}{T}(x_1, x_2)$, one can obtain the displacement functions ξ_1, ξ_2, η_1, and η_2. Their expressions are not displayed here.

Following the procedure used in Refs. 12–14, based on the extended Galerkin method, a nonlinear algebraic equation governing the postbuckling response is obtained and is expressed as

$$P_1[w_{pq}, \mathring{w}_{pq}, \underset{\sim}{N}_{11}, \underset{\sim}{N}_{22}] + P_2\left[w^2_{pq}, w_{pq}, \mathring{w}_{pq}\right]$$

$$+ P_3\left[w^3_{pq}, w^2_{pq}, w_{pq}, \mathring{w}_{pq}\right] + Q_1 \overset{1}{T}_{pq} + Q_2 q_{pq} = 0 \qquad (23)$$

where P_1, P_2, and P_3 are linear, quadratic, and cubic polynomials of the unknown modal amplitudes w_{pq} at the center of the panel and Q_1 and Q_2 are coefficients containing all of the data related to the geometry and thermomechanical properties of the sandwich structure. Because of their intricacy, these coefficients are not displayed here.

The relationship between the average applied compressive edge load and the average end shortening for predetermined temperature conditions is

$$\Delta_1 = \frac{-1}{(L_1 L_2)} \int_o^{L_1} \int_o^{L_2} \xi_{1,1} \, dx_1 \, dx_2 \qquad (24)$$

where Δ_1 is the dimensionless average end shortening in the x_1 direction.

The linearized counterpart of Eq. (23) results in a standard eigenvalue problem for the compressive edge loads whose solution yields the buckling load.

Numerical Simulations and Discussion

The displayed numerical results have the goal of highlighting the influence played by a number of effects on the buckling strength and the nonlinear response. These are supplied in both the International and U.S. Customary systems of units. The following materials with their thermomechanical characteristics and designations, displayed in Tables 1 and 2, were used to generate the results.

Effect of Panel Face Thickness on Compressive Buckling Strength and Results Comparisons

The effect of the thickness of each face sheet considered in conjunction with the distance a between the midplane of the core and the midplane of facings on the uniaxial compressive buckling strength is shown in Figs. 2 and 3. The top and bottom faces of the panel are constituted of three plies each, in the sequence [45/−45/45 deg]. $L_1 = L_2 = 9$ in. The face sheets and the core are made up from material F5 and C2, respectively (see Tables 1 and 2). Whereas in Fig. 2 all four edges are assumed to be movable, in Fig. 3 the two unloaded edges are considered to be immovable. In both cases, the results reveal that, with an increase of both the panel face thickness and of the parameter a, a continuous increase of the buckling strength is experienced. In the case of the immovability of the unloaded edges, a dramatic decrease of the buckling strength as compared to that of the panel counterpart featuring movable edges is experienced. Similar results to those in Fig. 2 have been provided by Pearce and

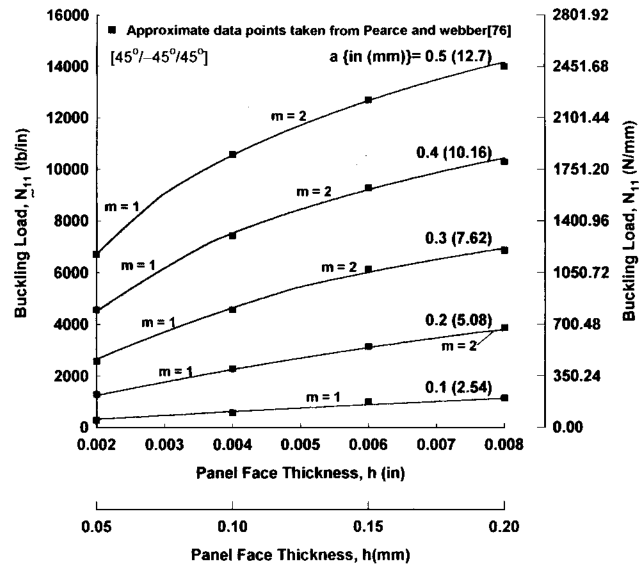

Fig. 2 Dependence of the uniaxial buckling load vs face thickness for selected values of the distance between the local midplane of the upper/lower face sheets and the midplane of the core.

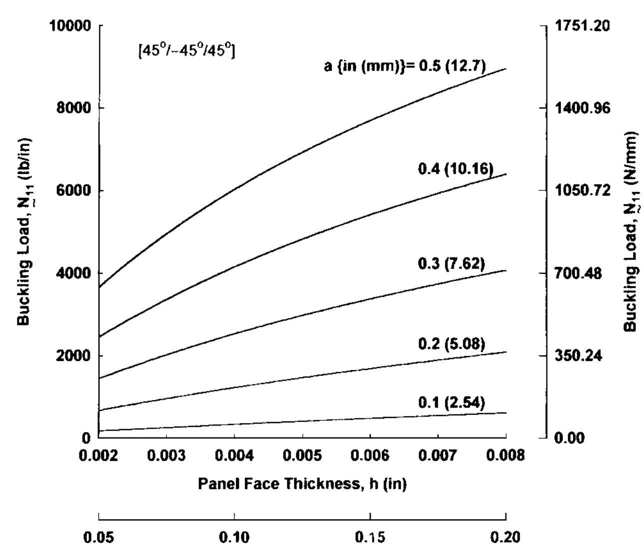

Fig. 3 Counterpart of Fig. 2 for the case where the unloaded edges ($x_2 = 0, L_2$) are immovable.

Webber.[2] Several approximate data points extracted from their analytical results (filled squares in Fig. 2) and plotted against the present ones reveal close agreement.

Effect on Buckling Strength of Fiber Orientation, in Conjunction with Panel Aspect Ratio

The variation of the buckling load vs ply angle for a flat sandwich panel characterized by selected values of its aspect ratio $\psi(\equiv L_2/L_1)$ is displayed in Fig. 4. Similar to the case considered in Ref. 7, the panel consists of a titanium honeycomb core (C1) and laminated angle-ply face sheets, each one made up from four laminas of material F3, in the sequence $[\theta/-\theta/-\theta/\theta]$. All edges

Table 3 Maxima for the buckling loads and the associated ply angles for different layups of face sheets

	ψ[a]				
Layup	0.9	1	1.2	1.4	1.6
(θ)	(11.5339)[48.6]	(9.3289)[45]	(6.8129)[37]	(5.567)[30.6]	(5.0144)[16.2]
$(\theta/-\theta/\theta)$	(11.8650)[47]	(9.5590)[44.1]	(6.9455)[38.6]	(5.6496)[31.5]	(5.0483)[19.8]
$(\theta/-\theta/\theta/-\theta/\theta)$	(11.894)[47.7]	(9.577)[45]	(6.9558)[38.7]	(5.6560)[31.5]	(5.0511)[19.8]

[a]Sequence ( )[ ] ≡ $(N_{11} \times 10^3)[\theta \text{ deg}]$ indicates the maximum buckling load (lb/in.) and the associated ply angle corresponding to the indicated layup and panel aspect ratio.

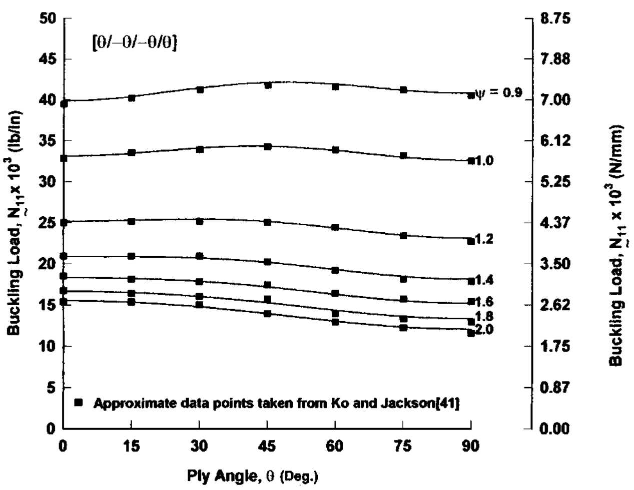

Fig. 4 Influence of the fiber orientation in the face sheets on the uniaxial buckling strength of a flat sandwich panel.

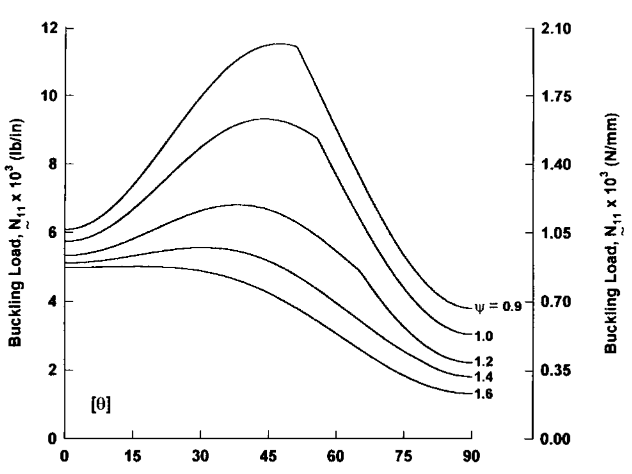

Fig. 5 Influence of the fiber orientation in the face sheets on the uniaxial compressive buckling strength of a sandwich panel.

are movable ($L_1 = 24$ in., $h_f = 0.032$ in., and $h_c = 0.584$ in.). Several data points extracted from the results of Ref. 7 (filled squares in Fig. 4) are plotted against the present ones, and they show a very close agreement. The results of Fig. 4 reveal a very low sensitivity of the buckling load to the variation of the fiber orientation in the face sheets. This trend is attributed to the very low orthotropicity ratio of the material used for the face sheets.

The results from Fig. 4 also reveal that for a panel of aspect ratio $\psi = 0.9$, the peak buckling load occurs approximately at a ply angle of $\theta = 50$ deg, whereas for a panel of aspect ratio $\psi = 1$, the peak buckling load appears to occur approximately at a ply angle of $\theta = 45$ deg. Furthermore, one can conclude that as the panel aspect ratio ψ increases, the angle ply at which the peak buckling load occurs is shifted toward lower ply-angles.

In Figs. 5 and 6 the variation of the buckling load as a function of ply angle for a sandwich panel of various aspect ratios is shown. In both cases the panel consists of an aluminum honeycomb core (C1)

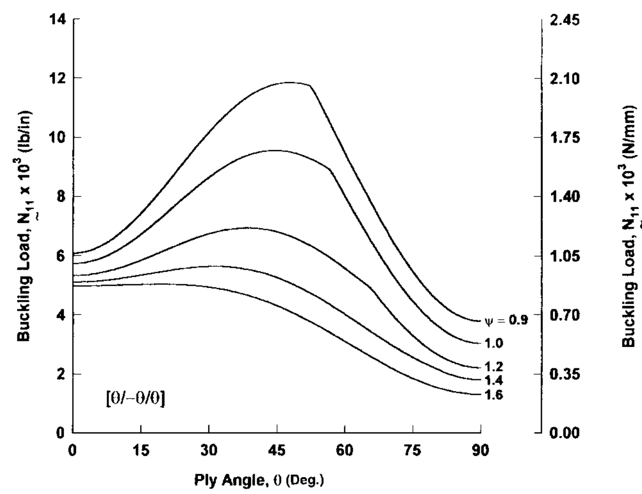

Fig. 6 Counterpart of Fig. 5.

and facings made up from HS graphite epoxy (F1). As is readily seen, the selected material of the face sheets is characterized by a rather large orthotropicity ratio. Each face of the sandwich panel considered in Fig. 5 is made up from one layer, in contrast to the panel in Fig. 6, for which each face consists of three plies in the sequence $[\theta/-\theta/\theta]$. In Fig. 5, all four edges are movable. It is also assumed that in both cases the thickness of face sheets remains unchanged ($L_1 = 24$ in., $h_f = 0.02$ in., and $h_c = 0.5$ in.). From Figs. 5 and 6, it becomes evident that for any considered panel aspect ratio, an increase of the number of layers in each face, without the increase of their thickness, is accompanied by a slight increase of the buckling strength. This trend becomes more evident from Table 3, where the first two considered sandwich panels are identical with those described in Figs. 5 and 6, whereas the third one, has the top and bottom face sheets made up of five layers in the sequence $[\theta/-\theta/\theta/-\theta/\theta]$. For all of these three considered panels, the thickness of face sheets is the same. The results shown in Figs. 5 and 6 also reveal that for aspect ratios $\psi \leq 1$, the buckling strength is more sensitive to the variation of ply angle than for panels of aspect ratio $\psi > 1$. In addition, from both Figs. 5 and 6 and Table 3, it becomes apparent that with the increase of the panel aspect ratio, both a decay of the maximum buckling strength and a shift of the corresponding ply angle toward smaller angles are experienced.

Notice that in Figs. 5 and 6, for any $\psi \leq 1.2$, the minimum buckling load prior to the first discontinuities have been determined for $m = n = 1$, whereas the remaining parts of the curves have been determined for $m = 2$, $n = 1$. However, for $\psi > 1.2$, there are no changes in the mode number for the minimum buckling load, that is, in this case this condition is obtained throughout for $m = n = 1$.

In Fig. 7, the case of sandwich panels whose face sheets are made up from three layers arranged in the sequence $[\theta/-\theta/\theta]$ was considered. For this case, it was assumed that the thickness of each constitutent ply is $h_p = 0.02$ in. With the exception that in this case the face sheets are three times thicker than in Fig. 6, the remaining mechanical and geometrical characteristics are identical.

The comparison of the results from Figs. 6 and 7 reveal that the increase in the thickness of face sheets results in a tremendous increase of the buckling strength. In addition, as compared to Fig. 6, Fig. 7 reveals that, besides the significant beneficial effect on the buckling strength resulting from the increase in face-sheet thickness,

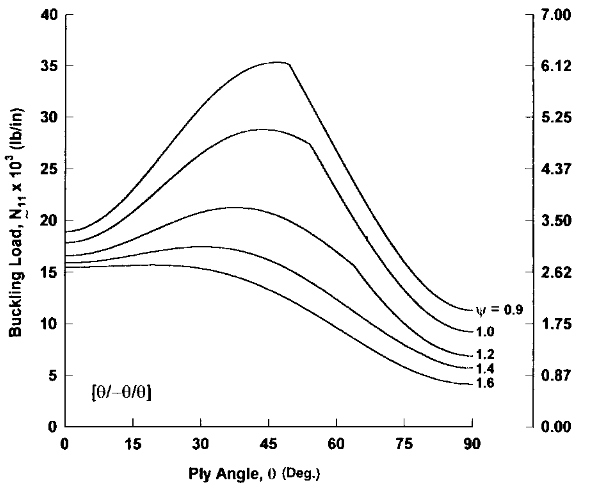

Fig. 7 Counterpart of Fig. 6, where each of the face sheets is three times thicker than in Fig. 6.

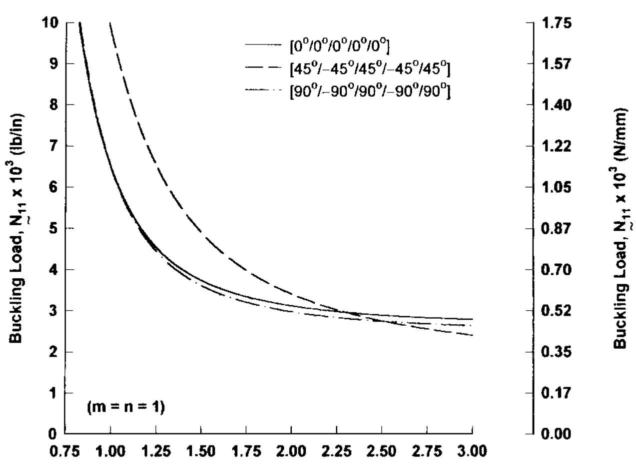

Fig. 8 Uniaxial buckling load vs panel aspect ratio for a flat sandwich panel.

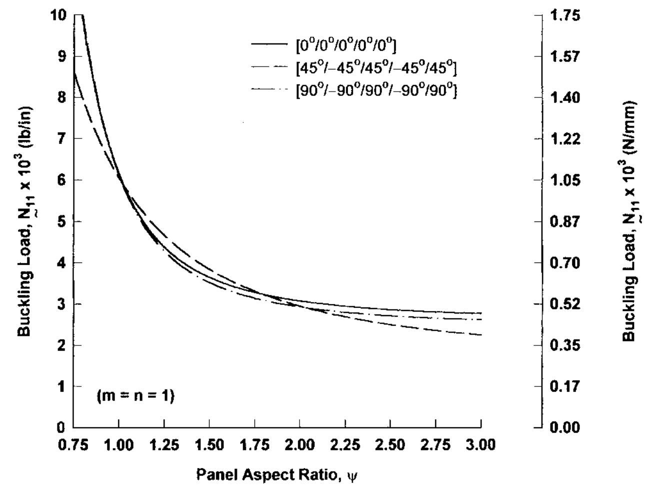

Fig. 9 Counterpart of Fig. 8 for the case of two immovable unloaded edges.

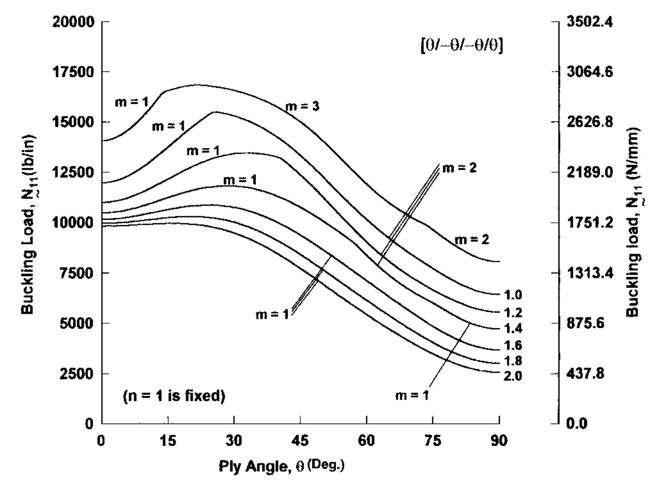

Fig. 10 Influence of fiber orientation in the face sheets considered in conjunction with that of the aspect ratio on the uniaxial compressive buckling of a sandwich panel.

no notable differences regarding implications of the aspect ratio coupled with that of the ply angle, as well as of the mode number rendering the minimum buckling load, can be reported.

Effect on Buckling Strength of Panel Aspect Ratio, in Conjunction with Selected Layups

In Fig. 8, the variation of the buckling load as a function of the panel aspect ratio is presented. In Fig. 8, L_1 = 24 in., h_f = 0.025 in, and h_c = 0.5 in. and the materials are F2 and C1. All edges are freely movable. The panel is considered to be uniaxially compressed, and each face sheet is made up of five laminae in three different layups. In all of these cases, a strong decrease of the buckling strength as a result of the increase in the panel aspect ratio is experienced. The [90/ −90/ 90/ −90/ 90 deg] layup appears to exhibit the lowest buckling strength up to an aspect ratio ψ = 2.4, beyond which the [45/ −45/ 45/ −45/ 45 deg] layup exhibits the lowest buckling load. This latter layup also exhibits the largest buckling strength of the three layups, up to an aspect ratio of $\psi \cong 2.4$. For aspect ratios greater than $\psi \cong 2.4$, the [0/0/0/0/0] layup yields the largest buckling strength.

Figure 9 represents the counterpart of Fig. 8 in the sense that, for this case, the unloaded edges are considered to be immovable. The buckling loads appear to occur at smaller values than for the case of all four edges being movable. This difference appears to be more pronounced at smaller aspect ratios, as opposed to the larger aspect ratios. The decay of the buckling strength for panels featuring immovable edges is attributed to the buildup of compressive stresses in the unloaded direction. A similar trend emerges also when comparing the results in Fig. 3 with their counterpart obtained for a panel featuring movable edges, Fig. 2. In addition, the [0/0/0/0/0] and [90/ −90/ 90/ −90/ 90 deg] layups relative to one another reveal the same trend of variation as in the case of all four edges being movable. In contrast to the case of all four edges being movable, in this case the [45/ −45/ 45/ −45/ 45 deg] layup features the least buckling strength of the three layups, up to the aspect ratio panel $\psi \cong 1$, beyond which this layup exhibits the largest buckling load capacity to an aspect ratio of $\psi \cong 1.75$. Finally, from an aspect ratio panel $\psi \cong 2.1$, this layup features the lowest buckling strength.

Effect on Buckling Strength of Transverse Shear Properties of the Core

Figures 10 and 11 show the uniaxial buckling response for a sandwich panel whose face sheets are constituted each of four plies in the sequence $[\theta/-\theta/-\theta/\theta]$. In Figs. 10 and 11, L_1 = 24 in., h_f = 0.08 in., and h_c = 0.5 in. All edges are freely movable. The only difference consists of the mechanical constants for the core. In Fig. 10 the core is made up from material C3, and in Fig. 11 from material C1. The results allow to infer the implications of transverse shear stiffness characteristics of the core on the buckling strength of uniaxially compressed sandwich panel. The results reveal the powerful role played by transverse shear stiffness characteristics, whose increase is associated with a significant increase of the buckling strength. In addition, as the results of Fig. 11 compared with those of Fig. 10 reveal, an increase of the ratio of the core transverse shear moduli $\bar{G}_{13}/\bar{G}_{23}$ tends to shift the occurrence of the maximum buckling load toward larger ply angles and also to yield larger variations of the buckling loads vs the ply angle as compared to the case of lower ratios of transverse shear moduli.

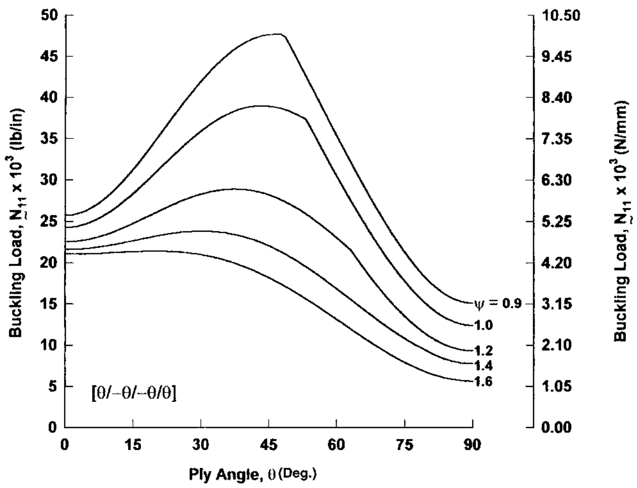

Fig. 11 Counterpart of Fig. 10 for the case of the core made of material C1.

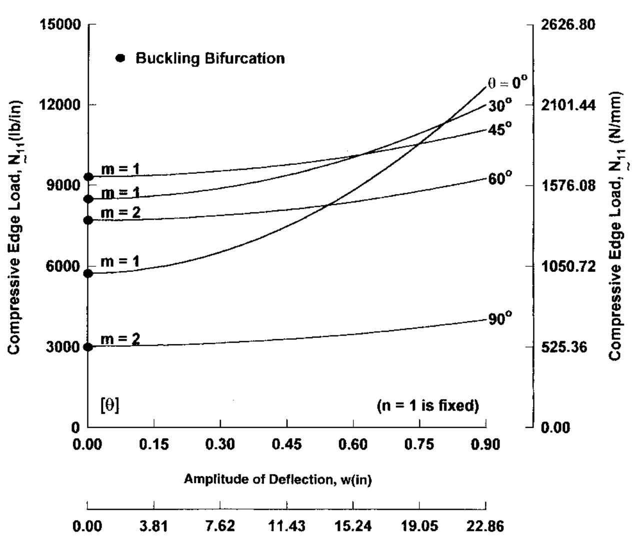

Fig. 12 Load-deflection amplitude interaction for a uniaxially compressed flat sandwich panel, whose face sheets are made up each from one layer.

Postbuckling Response of Sandwich Panels

The effect of the ply angle of the material of the face sheets on the edge load-center deflection interaction of a uniaxially compressed sandwich panel is shown in Fig. 12. Herein the top and bottom face sheets are made up of a single layer, each of the material F1. $L_1 = L_2 = 24$ in., $h_f = 0.02$ in., and $h_c = 0.5$ in. All edges are freely movable.

The results reveal that the buckling bifurcation loads identified by the filled circles on the ordinate increase to ply angle of 45 deg, after which, as the ply-angles increases, the buckling load decreases. A similar trend can be seen in the deep postbuckling range, where as the ply angles increase, the load-carrying capacity of the panel decreases. For the Fig. 12 case, a titanium honeycomb core (C1), which exhibits the largest transverse shear moduli among the materials from Table 2, was considered.

In Fig. 13 the aluminum honeycomb (C3) characterized by much lower transverse shear stiffness characteristics is used for the core, and the considered thickness of face sheets is more than double that in Fig. 12. The results shown in Fig. 13 reveal that the two effects that are contradictory in nature, namely, increase of thickness of face sheets, on one hand, and decrease of transverse shear moduli of the core, on the other hand, compensate each other, so that finally the buckling strength and load-carrying capacity in the postbuckling range remain roughly unchanged. However, because the ratio $\bar{G}_{13}/\bar{G}_{23}$ is lower in the latter case, a more reduced sensitivity of both

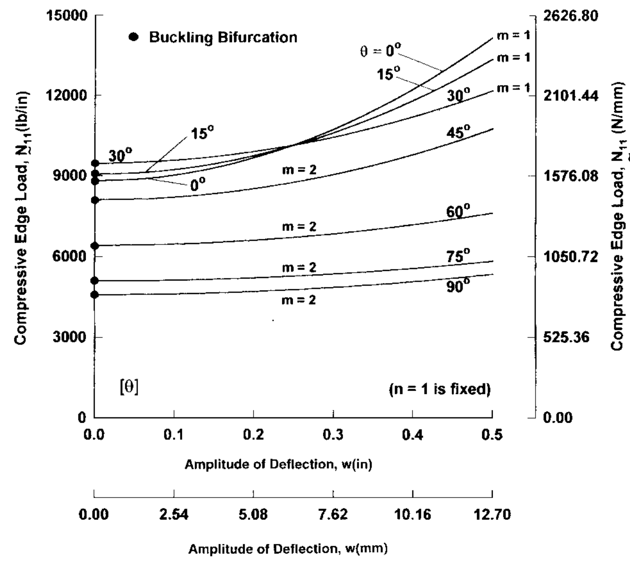

Fig. 13 Counterpart of Fig. 12 for the case of the core made of the material C3, with top and bottom face sheets of thickness h_f = 0.05 in.

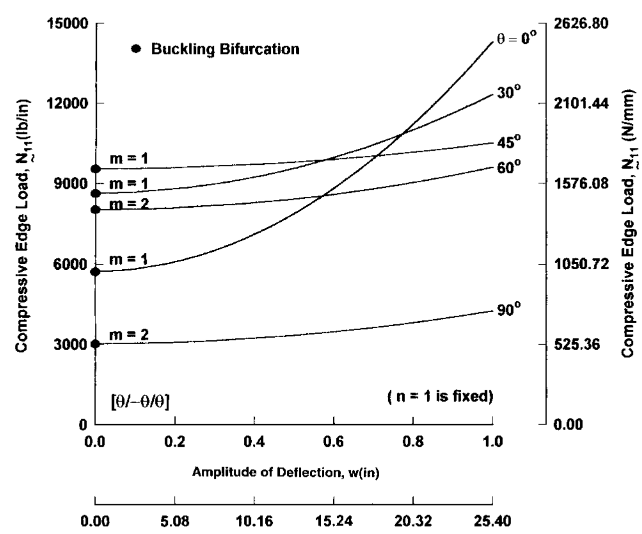

Fig. 14 Counterpart of Fig. 12, for the case of face sheets constituted each of three layers whose total thickness is equal with that in Fig. 12.

the buckling strength and load-carrying capacity in the postbuckling range to the variation of the ply angle is experienced. Moreover, consistent with what was remarked when the results of Fig. 11 were compared with those of Fig. 10, in this case the decrease of the ratio $\bar{G}_{13}/\bar{G}_{23}$ results in a shift of the buckling loads toward lower ply angles and less sensitivity of the buckling and load-carrying capacity to the ply angle variation.

In Fig. 14, the panel features the same geometrical and mechanical characteristics as in Fig. 12, excepting that each face is made up of three layers in the sequence $[\theta/-\theta/\theta]$. In spite of this, their thickness is the same as for one layer, that is, as in Fig. 12. The same type of behavior can be seen in the deep postbuckling range but differs at the buckling bifurcation. It is revealed that, at the smaller ply angles, the buckling bifurcation as well as the load-bearing capacity are a little larger as opposed to the trend appearing in Fig. 12.

The increase of face-sheet thickness yields a dramatic increase of both the buckling loads and load-carrying capacity in the postbuckling range. In contrast to Fig. 14, Fig. 15 shows the same conditions and interactions but for a larger face-sheet thickness; now the thickness of each of the face sheets is three times larger than that corresponding to Fig. 14. In spite of this modification, no change in the behavior as compared to that in Fig. 14 is emerging; as the ply angles increase, in the deep postbuckling range the load-carrying capacity

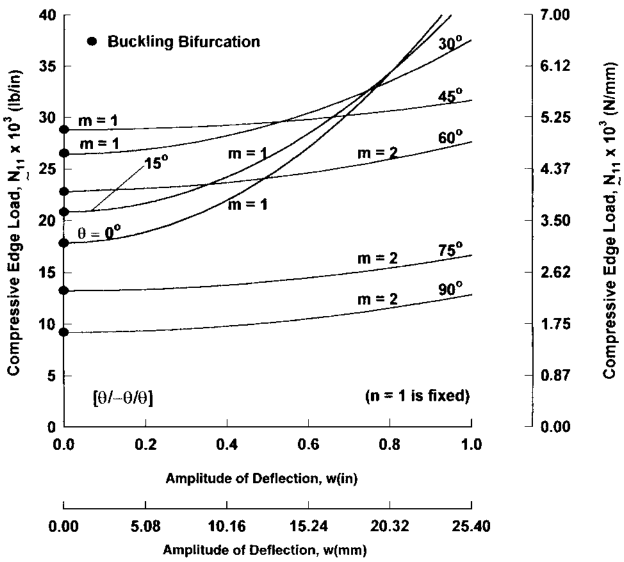

Fig. 15 Counterpart of Fig. 14 for the case of face sheets made up from three layers whose thickness is three times that in Fig. 14.

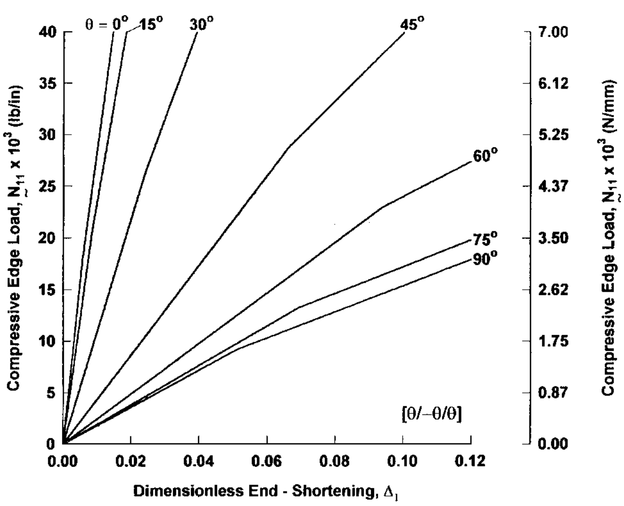

Fig. 16 Counterpart of Fig. 14 depicting the load–end-shortening dependence.

of the panel decreases. The counterpart of Fig. 15 portraying the load–end-shortening interaction is shown in Fig. 16. The results of Fig. 16 reveal that, as the ply angle increases, the end shortening increases as well. For fixed compressive edge loads, at lower ply angles, much smaller end shortenings than at larger ply angles are experienced.

Figure 17 representing the counterpart of Fig. 15, corresponds to the case of panels featuring two immovable unloaded edges. For this case it is revealed that the buckling occurs at much lower compressive loads for all considered ply-angle configurations. In addition, it is apparent that the maximum buckling bifurcation occurs at the ply angle $\theta = 30$ deg, as opposed to $\theta = 45$ deg, as seen earlier in the case of all four edges being movable. Moreover, in contradistinction with the case of all edges being movable, in this case, at larger ply angles, for example, $\theta = 60$, 75, and 90 deg, the sensitivity of the variation of buckling strength and load-carrying capacity with that of ply angle is almost nonexistent.

Figure 18 showing the load–end-shortening dependence represents the counterpart of Fig. 17. Figure 18 reveals that for a given compressive edge load, at large ply angle, the end shortening is larger than for smaller ply angles. In addition, it is also shown that, in contrast to the case of all four edges being movable, in the case of two immovable unloaded edges the buckling bifurcation occurs at much smaller magnitudes of the end shortening.

Figure 19 shows the case of a flat sandwich panel whose top and bottom face sheets are made up each from three (of the material F1)

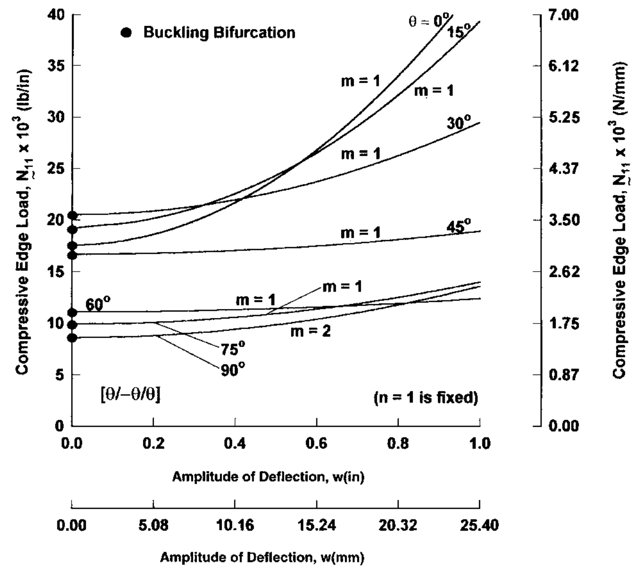

Fig. 17 Counterpart of Fig. 15 for the case of the immovable unloaded edges.

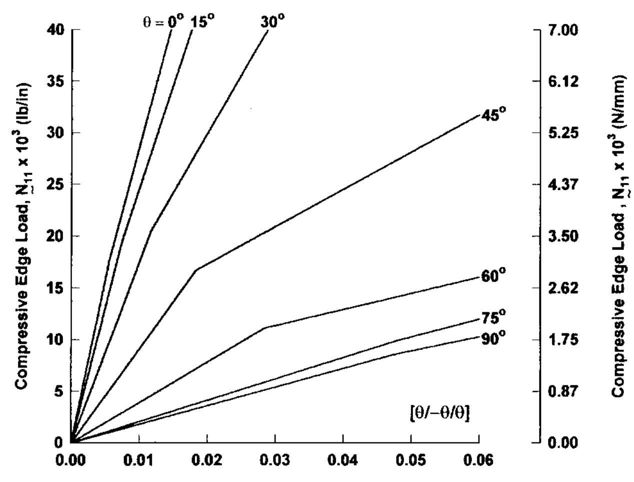

Fig. 18 Load–end-shortening interaction for the case considered in Fig. 17.

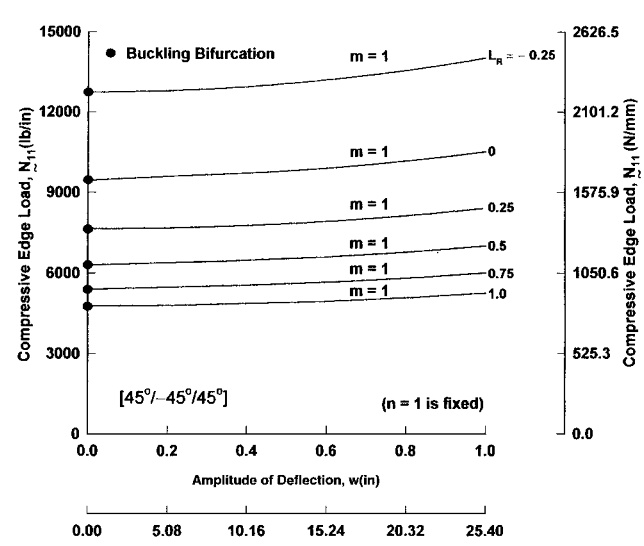

Fig. 19 Postbuckling response of a sandwich panel under biaxial compression/tension.

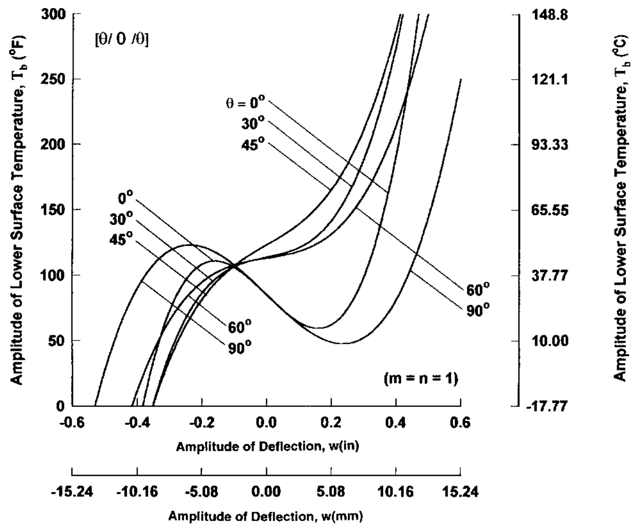

Fig. 20 Nonlinear response of a sandwich geometrically imperfect flat panel.

layers in the sequence [45/ −45/ 45 deg], whereas the core is of the material C1. $L_1 = L_2 = 24$ in., $h_f = 0.02$ in., and $h_c = 0.5$ in. All edges are freely movable. The panel is considered to be subjected to the compressive load $\underset{\sim}{N}_{11}$ on the edges $x_1 = 0, L_1$ and to the compressive/tensile loads $\underset{\sim}{N}_{22}$ on the edges $x_2 = 0, L_2$. As a result, the edge load ratio $L_R (\equiv \underset{\sim}{N}_{22}/\underset{\sim}{N}_{11})$ is $L_R > 0$, $L_R = 0$, and $L_R < 0$, depending on whether $\underset{\sim}{N}_{22} > 0$ (corresponding to compression), $\underset{\sim}{N}_{22} = 0$, or $\underset{\sim}{N}_{22} < 0$ (corresponding to tension), respectively. One supposes that the compressive load $\underset{\sim}{N}_{11}$ increases gradually. The results reveal that a considerable increase of the buckling strength is achieved by applying an increased tension on the edges $x_2 = 0, L_2$. The same can be inferred about the postbuckling behavior. In contradistinction with this case, when all of the edges are subjected to compressive loads, a decrease of the buckling strength is experienced.

Effects of the Combined Compressive Edge Load and Temperature

In Fig. 20 one considers the case of flat sandwich panels whose top and bottom faces are made up from three layers of equal thickness in the sequence $[\theta/0/\theta$ deg]. The material of the face sheets is F1 and the core is C3. $L_1 = L_2 = 24$ in., $h_f = 0.01125$ in., and $h_c = 0.35$ in. All edges are freely movable. The panel is exposed to an antisymmetric temperature gradient through the panel thickness, the temperature amplitude on the bottom plane, T_b, is assumed to be positive. This implies that the temperature field $T(x_1, x_2, x_3) = x_3(2/H)T_b(x_1, x_2)$. It is assumed that the panel features an upward initial geometric imperfection, $\overset{\circ}{w} = -0.0875$ in. and that the edges $x_1 = 0, L_1$, are subjected to the compressive preload $\underset{\sim}{N}_{11} = 1850$ lb/in. The results reveal that under these conditions, for $T_b = 0$, the panel exhibits a negative (upward) initial deflection. With the increase of T_b, the deflection becomes gradually less negative; for a certain T_b, depending on the ply angle, a limit temperature is reached, which, by further increase of T_b, is followed by a snap-through buckling. At the same time, the results reveal that for some ply angles, for example $\theta = 30$, 45, and 60 deg, the intensity of the snap through can dramatically be attenuated and can even be eliminated altogether, for example, for $\theta = 45$ deg.

Conclusions

The results presented concern the behavior of sandwich flat panels with anisotropic face sheets subjected to uni/biaxial edge loads and an antisymmetric through panel wall-thickness temperature gradient. The material of each constituent lamina of the face sheets was considered to feature anisotropic properties induced by the rotation of the fibers in each constituent ply with respect to the axes of the structure. With the generation of stiffness quantities $A_{\alpha 6}$ and $D_{\alpha 6}$, $(\alpha = 1, 2)$, induced by this off-axis material configuration, an increase in the buckling strength and postbuckling is experienced, The results indicate that the directionality property of facings can play a tremendous role toward enhancing the buckling strength and the load-carrying capacity in the postbuckling range. The implications of immovability of unloaded edges and of elastic characteristics of materials of face sheets and of the core on the buckling and postbuckling strength have also been highlighted, and their important role in enhancing the buckling strength and the postbuckling response behavior was emphasized.

Moreover, it was shown that in some complex loading conditions, when also flat sandwich panels can experience snap-through buckling, a judicious use of the directional properties of the material of face sheets can result in the attenuation of its intensity and even in its elimination altogether.

Appendix: Strain-Displacement Relationships

Bottom face sheets:

$$'\varepsilon_{11} = \xi_{1,1} + \eta_{1,1} + \tfrac{1}{2}v_{3,1}^2 + v_{3,1}\overset{\circ}{v}_{3,1} \qquad (1 \rightleftarrows 2)$$

$$'\gamma_{12} = \xi_{1,2} + \xi_{2,1} + \eta_{1,2} + \eta_{2,1} + v_{3,1}v_{3,2} + \overset{\circ}{v}_{3,1}v_{3,2} + v_{3,1}\overset{\circ}{v}_{3,2}$$

$$'\kappa_{11} = -v_{3,11} \qquad (1 \rightleftarrows 2)$$

$$'\kappa_{12} = -2v_{3,12}$$

Core layer:

$$\bar{\varepsilon}_{11} = \xi_{1,1} + \tfrac{1}{2}v_{3,1}^2 + \overset{\circ}{v}_{3,1}v_{3,1} \qquad (1 \rightleftarrows 2)$$

$$\bar{\gamma}_{12} = \xi_{1,2} + \xi_{2,1} + v_{3,1}v_{3,2} + \overset{\circ}{v}_{3,1}v_{3,2} + v_{3,1}\overset{\circ}{v}_{3,2}$$

$$\bar{\kappa}_{11} = \frac{1}{h}\left\{\eta_{1,1} + \frac{1}{2}hv_{3,11}\right\} \qquad (1 \rightleftarrows 2)$$

$$\bar{\kappa}_{12} = \frac{1}{h}\{\eta_{1,2} + \eta_{2,1} + hv_{3,12}\}$$

$$\bar{\gamma}_{13} = \frac{1}{h}\left\{\eta_1 + \frac{1}{2}hv_{3,1}\right\} + v_{3,1} \qquad (1 \rightleftarrows 2)$$

Top face sheets:

$$''\varepsilon_{11} = \xi_{1,1} - \eta_{1,1} + \tfrac{1}{2}(v_{3,1})^2 + \overset{\circ}{v}_{3,1}v_{3,1} \qquad (1 \rightleftarrows 2)$$

$$''\gamma_{12} = \xi_{1,2} + \xi_{2,1} - \eta_{1,2} - \eta_{2,1} + v_{3,1}v_{3,2} + \overset{\circ}{v}_{3,1}v_{3,2} + v_{3,1}\overset{\circ}{v}_{3,2}$$

$$''\kappa_{11} = -v_{3,11} \qquad (1 \rightleftarrows 2)$$

$$''\kappa_{12} = -2v_{3,12}$$

Acknowledgment

The work reported herein was supported in part by NASA Langley Research Center under Grant NAG-1-1689.

References

[1]Noor, A. K., Burton, W. S., and Bert, C. W., "Computational Model for Sandwich Panels and Shells," *Applied Mechanics Reviews,* Vol. 4, No. 3, 1996, pp. 155–199.

[2]Pearce, T. R. A., and Webber, J. P. H., "Buckling of Sandwich Panels with Laminated Face Plates," *Aeronautical Quarterly*, Vol. 24, Nov. 1973, pp. 295–331.

[3]Rao, K. M., "Buckling Analysis of Anisotropic Sandwich Plates Faced with Fiber-Reinforced Plastics," *AIAA Journal*, Vol. 23, No. 8, 1985, pp. 1247–1253.

[4]Kim, C. G., and Hong, C. S., "Buckling of Unbalanced Anisotropic Sandwich Plates with Finite Bonding Stiffness," *AIAA Journal*, Vol. 26, No. 8, 1988, pp. 982–988.

[5]Rao, K. M., and Meyer Piening, H. R., "Buckling Analysis of FRP-Faced Cylindrical Sandwich Panels Under Combined Loadings," *Composite Structures*, Vol. 14, 1990, pp. 15–34.

[6]Ko, W. L., and Jackson, R. H., "Combined-Load Buckling Behavior of Metal-Matrix Composite Sandwich Panels Under Different Thermal Environments," NASA TM 4321, Sept. 1991.

[7]Ko, W. L., and Jackson, R. H., "Compressive and Shear Buckling Analysis of Metal Matrix Composite Sandwich Panels Under Different Thermal Environments," *Composite Structures*, Vol. 25, 1993, pp. 227–239.

[8]Librescu, L., Hause, T., and Camarda, C. J., "Geometrically Nonlinear Theory of Initially Imperfect Sandwich Plates and Shells Incorporating Nonclassical Effects," *AIAA Journal,* Vol. 35, No. 8, 1997, pp. 1393–1403.

[9]Hause, T., Librescu, L., and Camarda, C. J., "Postbuckling of Anisotropic Flat and Doubly-Curved Sandwich Panels Under Comples Loading Conditions," *International Journal of Solids and Structures*, Vol. 35, No. 23, 1998, pp. 3007–3028.

[10]Librescu, L., *Elastostatics and Kinetics of Anisotropic and Heterogeneous Shell-Type Structures*, Noordhoff International, Leyden, The Netherlands, 1975, Chaps. 5–7, pp. 493–540.

[11]Librescu, L., "Refined Geometrically Non-Linear Theories of Anisotropic Laminated Shells," *Quarterly of Applied Mathematics*, Vol. 45, No. 1, 1997, pp. 1–22.

[12]Hause, T., Librescu, L., and Johnson, T. F., "Nonlinear Response of Geometrically Imperfect Flat and Curved Sandwich Panels Subjected to Thermomechanical Loading," *International Journal of Non-Linear Mechanics*, Vol. 33, No. 6, 1998, pp. 1039–1059.

[13]Librescu, L., and Stein, M., "Postbuckling of Shear Deformable Composite Flat Panels Taking into Account Geometrical Imperfections," *AIAA Journal*, Vol. 30, No. 5, 1992, pp. 1352–1360.

[14]Librescu, L., Lin, W., Nemeth, M. P., and Starnes, J. H., Jr., "Classical Versus Non-Classical Postbuckling Behavior of Laminated Composite Panels Under Complex Loadings Conditions," *Non-Classical Problems of the Theory and Behavior of Structures Exposed to Complex Environmental Conditions*, edited by L. Librescu, Vol. 164, American Society of Mechanical engineers, Fairfield, NJ, 1993, pp. 169–182.

[15]Seide, P., "A Reexamination of Koiter's Theory of Initial Postbuckling Behavior and Imperfection Sensitivity of Structures," *Thin Shell Structures: Theory, Experiment and Design*, edited by C. Y. Fung and E. E. Sechler, Prentice–Hall, Upper Saddle River, NJ, 1974, pp. 59–80.

[16]Simitses, G. J., "Buckling and Postbuckling of Imperfection Cylindrical Shells: A Review," *Applied Mechanics Reviews*, Vol. 39, No. 10, 1986, pp. 1517–1524.

H. L. McManus
Associate Editor